HHS Public Access

Author manuscript

Biomaterials. Author manuscript; available in PMC 2020 March 25.

Published in final edited form as:

Biomaterials. 2019 March ; 197: 296–304. doi:10.1016/j.biomaterials.2019.01.027.

Engineered Bone for Probing Organotypic Growth and Therapy Response of Prostate Cancer Tumoroids *in vitro*

Claudia Paindelli[a,b], **Nora Navone**[a], **Christopher J. Logothetis**[a], **Peter Friedl**[a,b,c], **Eleonora Dondossola**[a,*]

[a]David H. Koch Center for Applied Research of Genitourinary Cancers, The University of Texas MD Anderson Cancer Center, 1515 Holcombe Blvd, 77030, Houston, TX USA [b]Radboud University Nijmegen, Nijmegen, Geert Grooteplein 26, 6500 HB Nijmegen, The Netherlands [c]Cancer Genomics Centre (CGC.nl), 3584 Utrecht, The Netherlands

Abstract

Mechanistic analysis of metastatic prostate cancer (PCa) biology and therapy response critically depends upon clinically relevant three-dimensional (3D) bone-like, organotypic culture. We here combine an engineered bone-mimetic environment (BME) with longitudinal microscopy to test the growth and therapy response of 3D PCa tumoroids. Besides promoting both tumor-cell autonomous and microenvironment-dependent growth in PCa cell lines and patient-derived xenograft cells, the BME enables *in vivo*-like tumor cell response to therapy, and reveals bone stroma dependent resistance to chemotherapy and BME-targeted localization and induction of cytoxicity by Radium-223. The BME platform will allow the propagation, compound screening and mechanistic dissection of patient-derived bone tumor isolates and applications toward personalized medicine.

Keywords

prostate cancer; bone metastasis; in vitro engineered bone microenvironment; therapy response; 3D culture; microscopy

1. Introduction

Bone metastases cause detrimental complications in patients with advanced cancers, including prostate cancer (PCa), with limited therapeutic options to eliminate once-established bone lesions [1, 2]. Besides cell intrinsic drivers, including up-regulation of secreted cytokines and surface receptors, the bone microenvironment critically contributes to progression, therapy response and resistance development of metastatic PCa in bone [1, 2].

*Corresponding author, EDondossola@mdanderson.org; Fax number, 713-792-6599.

Contributions: C.P., E.D., N.N., C.J.L. and P.F. designed research; N.N. provided PDXs; C.P. and E.D. performed research; C.P., N.N, P.F. and E.D. analyzed data; C.P., E.D. and P.F. wrote the paper; all authors read and corrected the manuscript.

Competing interests: The authors declare that they have no competing interest.

Data availability: The authors declare that all the relevant data supporting the findings of this study are available within the paper and its supplementary information, and from the corresponding authors upon reasonable request.

Traditionally, both PCa biology and response to therapeutics, *in vitro,* have been tested in cancer cell lines grown in 2D plastic dishes [3, 4]. These cultures, however, lack both the matrix and multicellular composition of bone, which limits their relevance for addressing cancer-bone cell interplays and resulting outcomes [5]. As bone-mimetic systems, engineered *in vitro* models enable to combine stromal cells, including mesenchymal precursors, endothelial cells, osteoblasts and osteoclasts, with 3D geometry and a calcified extracellular matrix and allow further co-culture with cancer cells [6]. These engineered platforms include (i) bone-derived cells in bioreactors [7]; (ii) matrix-based 3D hydrogels or collagen mono- and co-cultures [6, 8]; (iii) synthetic or natural 3D scaffolds seeded with stromal cells that develop ossified bone-like 3D structures [9, 10]; microfluidic devices [11] and (iv) explanted bone [12]. Such models reveal defined cancer/bone interactions and fundamental principles of bone cancer biology, including growth, survival, extravasation, adhesive and paracrine cell-cell interactions and androgen sensitivity [3, 6–8, 10–12]. Besides these cellular functions, the more physiological cell organization and enriched signaling response sustained by engineered 3D cultures can profoundly affect sensitivity/resistance to treatments ([4, 13]). However, *in vitro* engineered bone models have been occasionally applied for probing the therapy response ([14, 15]) and underlying mechanism of resistance ([9]).

We here developed 3D long-term culture of multicellular tumoroids in bone-mimetic environments (BME) and apply live-cell microscopy to study their growth and response to therapy. Our data reveal a critical contribution of the BME to provide topologic niches of therapy response heterogeneity and cancer cell resistance (Fig. 1).

2. Materials and Methods

2.1 Cell line cultures and reagents

Human dual-color variant PC3 prostate cancer cells expressing H2B-eGFP and DsRed2 were from Anticancer; luciferase-expressing PC3 cells were provided by Dr. Gary Gallick, UT MD Anderson Cancer Center. Cells were maintained in DMEM (Corning), 10% fetal calf serum (Sigma), penicillin and streptomycin (both 100 μg/ml, Sigma). Human C4–2B cells (provided by Dr. Timothy Thompson, UT MD Anderson Cancer Center) expressing H2B/mCherry and LifeAct-GFP were cultured in RPMI (Corning), 10% fetal calf serum (Sigma), penicillin and streptomycin (both 100 μg/ml, Sigma) and 1% HEPES. The identity of tumor cell lines was verified by Short Tandem Repeat DNA profiling (Characterized Cell Line Core Facility, M.D. Anderson Cancer Center). ASC52telo telomerase reverse transcriptase immortalized adipose tissue derived mesenchymal stem cells (hMSCs, ATCC) were maintained in Minimum Essential Medium (MEM1X, Corning), supplemented with 17% fetal calf serum, vitamins (Sigma), non-essential amino acids (Sigma), sodium pyruvate (Gibco), penicillin and streptomycin (both 100 μg/ml, Sigma). To induce osteoblastic differentiation, hMSCs were cultured in osteogenic medium (DMEM 1X, supplemented with 10% calf serum, penicillin and streptomycin, 50 μg/ml L-ascorbic acid, 10 mM β-glycerophosphate, 0.1 μM dexamethasone from Sigma).

2.2. Patient-derived xenografts generation and processing

MDA PCa 118b and MDA PCa 183 patient derived xenografts (PDXs) were developed in the laboratory of Dr. Navone at the "Prostate Cancer Patient Derived Xenografts Program", department of Genitourinary Medical Oncology, MD Anderson Cancer Center and the David H. Koch Center for Applied Research of Genitourinary Cancers. PDXs were established following previous described procedures and propagated as subcutaneous xenografts in 6- to 8-week-old male NOD/SCID gamma male mice (Experimental Radiation Oncology, MD Anderson Cancer Center) [16–18]. Maintenance of PDXs in mice was approved by the Institutional Animal Care and Use Committee of The University of Texas MD Anderson Cancer Center. Tumors were harvested when reaching 1–2 cm^3, cut in small pieces (3–4mm^3) and mechanically disaggregated using the plunge of a 1 ml syringe on a cell strainer (100 μm pore size) in DMEM medium. Upon disaggregation of the mouse-derived tumor, MDA PCa 183 gave rise to larger and cohesive aggregates, while MDA PCa 118b generated smaller and looser clusters, in line with their *in vivo* pattern of growth [16–18]. To enrich for tumor cell clusters, the cell suspension was centrifuged in a Ficoll gradient (Lymphoprep, STEMCELL Technologies). To generate fluorescent PDX variants, freshly isolated cells (3.75×10^5 cells) were stably transduced with 1μl of rLV.EF1.mCherry-9 lentiviral vector (Vectalys) and 0.5 μl of Polybreene, in 1ml of DMEM complete medium in a 24-well plate (Thermo Fisher), overnight. PDXs-derived transduced cells were washed three times in PBS and seeded on the scaffolds (7.5×10^4 cells/well, 150 μl/well in a 96 wells plate).

2.3 mPCL-CaP scaffold fabrication

Medical grade PCL scaffolds were 3D printed by melt electrospinning writing and surface-treated with calcium phosphate coating, as described [19].

2.4 Generation and characterization of functionalized mPCL-scaffolds

hMSCs were detached from 2D culture at 70–80% confluence with trypsin-EDTA (Sigma), seeded on the scaffold (2.5×10^5 cells in 25 μl, 37 °C, 5% CO2, for 4h) and maintained in osteogenic medium. The seeding duration of 4h was sufficient to favor the interaction of the cells with the scaffold and subsequent homogenous colonization. Osteogenic medium was completely replaced weekly. To investigate 3D BME organization at 10, 20 or 30 days after seeding, BME culture was incubated overnight with xylenol orange (20μM in osteogenic medium; Sigma), rinsed in PBS, fixed (2% PFA, 30 min), and incubated with phallodin-Alexafluor488 (1:100; Invitrogen) and DAPI in staining solution (10% FBS, 0.2% triton X-100, 0.1% BSA in PBS). To detect collagen I, fixed BMEs were blocked in staining solution 1h, then incubated with anti-collagen I antibody (1:100 in staining solution; ab34710, AbCam) over night. BMEs were washed in PBS for 3 h (with several changes of PBS), incubated with goat anti rabbit Alexafluor647 antibody (1:200 in staining solution; Invitrogen) 4h, washed 3h in PBS and stained with DAPI. To detect alkaline phosphatase, fixed and blocked BMEs were incubated over night with anti-alkaline phosphatase Alexafluor488 antibody (1: 30; 561495, BD), washed 3 h in PBS and stained with DAPI.

2.5 Generation of PCa tumoroids and seeding on mPCL scaffolds

Tumoroids of PCa cells (PC3 and C4–2B) were generated with the hanging-drop method. Briefly, 10^5 PCa cells were incubated in 20% methyl cellulose in cell culture medium supplemented with 1% matrigel (BD Biosciences) and deposited as 25 μl drops on the lid of a 15 cm dish. The lid was inverted and the drops incubated overnight at 5% CO_2, 37 °C. After aggregation, PCa tumoroids were positioned in the center of mPCL-CaP or BME in a 96 well-plate and overlaid with DMEM/FCS (75μl). For precise tumoroid positioning, the bottom part of a 10μl tip was placed in the 96 well to facilitate the positioning of the tumoroids on a restricted scaffold area. 3D tumoroid cultures were incubated overnight at 37°C, 5% CO2, transferred to a 48-well plate and cultured in a 1:1 mixture of PCa cells/ osteogenic growth medium.

2.6 Image acquisition and quantitative analysis

Images from 3D stacks were reconstructed and analyzed using Fiji [20]. PCa tumoroid growth was monitored using an EVOS FL Cell Imaging System (AMG) equipped with 2X AMEP 4631 objective, NA=0.06. Tumoroid growth was quantified as fluorescent intensity, as the summation (∑) of the grey value of all the pixels. The area occupied by each tumoroid was defined as region of interest (ROI) with the magic wand tool. The background signal was determined as the mean gray value from a cell-free ROI (40×40 px) in the same position for all images and used for background subtraction as follows: fluorescent intensity tumoroids – (area tumoroid x mean grey background). All images were taken using the same setting at every time point.

PDXs growth and nuclear status during therapy response experiments with PC3 cells were recorded using a confocal Leica MST66 microscope equipped with a Leica Z6 APO zoom lens. PDX growth was quantified from the mCherry signal. Single channel z-stacks were masked, thresholded (Moments plug-in, FIJI) and the signal-positive area was obtained. For each sample, the relative fluorescence density was obtained averaging 10 slices per z-stack. Therapy response in different tumoroid regions, including core or dhMSC-interface areas, was scored by counting the number of apoptotic and non-apoptotic nuclei (based on nuclear fragmentation) detected by H2B-eGFP nuclear signal. Scaffold maturation analysis and orthogonal view of scaffolds seeded with PCa cells and PDXs were performed by using a TrimScope II (LVBT) equipped (LaVision BioTech) with three Ti:Sapphire lasers (Chameleon-XR, Coherent) and two Optical Parametric Oscillators (APE/Coherent), resulting in a tunable excitation range from 800 to 1,300 nm and up to three laser lines [21]. The microscope was equipped with a long-working distance 25x NA 1.05 oil/water (Olympus) objective. Simultaneous detection was performed using up to 5 backward photomultipliers, with spectral separation of channels for DAPI and THG (450/60, 1090 nm and 1280 nm), eGFP (525/50, 920 nm), SHG (525/50, 1090 nm), DsRed2 (595/40, 1090nm), xylenol orange and mCherry (620/60, 1090 nm). 3D stacks were obtained for up to 200 μm depth at 5–10 μm step-size. Images from individual 3D stacks were reconstructed and analyzed using FIJI. To analyze calcium deposition over time, xylenol orange signal was thresholded (Li plug-in, FIJI) in individual slices from 3D stacks (10 consecutive frames were averaged; 360 × 360 μm, 5 μm step interval in z-direction) and calculated as % of the total area.

2.7 Treatment of PC3 in 2D culture

For testing docetaxel toxicity, luciferase-expressing PC3 cells were cultivated in a 96-well plate (2000 cells/well) and treated after 1 d with docetaxel (0–100 nM, 1:3 dilutions, Sanofi). The growth was measured over time by bioluminescence signal using an automatic plate reader (PerkinElmer, EnVision 2104 multi label plate reader), after addition of luciferine solution (150μg/ml). For testing Radium-223 (Rad223) toxicity, luciferase-expressing PC3 cells were seeded in a 96-well plate (1500cells/well) and treated after 1 d with Rad223 (0–6400 Becquerel/ml, 1:2 dilutions, Bayer).

2.8 Treatment of PC3 in BME

To assess docetaxel toxicity in BME, PC3 tumoroids were seeded on BME and mPCL-CaP scaffolds, after 5 d treated with docetaxel and their growth monitored by epifluorescence microscopy. To evaluate Rad223 toxicity in BME, PC3 tumoroids were seeded on BME, after 3 d treated with Rad223 and their growth monitored overtime.

3. Results

3. 1 *In vitro* bone mimetic environment (BME)

As *in vitro* bone mimetic environment (BME), calcium phosphate-coated, medical grade polycaprolactone (mPCL-CaP) scaffolds in a micro format (5 × 5 × 0.2 mm; Fig. 2A, B) were colonized with human mesenchymal stem cells (hMSCs) and matured in osteo-inductive medium over 4 weeks (Fig. 1A; Fig. 2C) [22]. BMEs consisted of secretory osteogenic differentiated hMSCs (dhMSCs) extending along and intercalating between scaffold fibers (Fig 2. C–E) in a 3D niche-like fashion, as described [10, 23]. The density of hMSCs with intact nuclei remained unchanged over time (Fig. 2F), indicating a largely non-proliferative state. However, concomitant to osteogenic differentiation, calcium phosphate content increased over 30 days of culture, with focal deposits of calcified matrix in the inter-fiber space (Fig. 2G, asterisk), as well as collagen I deposition (Fig. 2H) and expression of alkaline phosphatase (Fig. 2I), typical of mature osteoblasts. To test whether the scaffold geometry impacts this osteogenic process, we compared mPCL-CaP scaffolds with different overall shapes and intrinsic microscopic properties, including thickness, number and distribution of fibers (Fig. S1A, B). Irrespective of the macro- and micro-geometry of the scaffolds, comparable density of colonization by hMSCs or calcium deposition were obtained (Fig. S1C, D). The G1 geometry was prioritized for further experiments because of its uniform topology, more suited for reliable central positioning of tumor cell suspensions and tumoroids.

Thus, we generated a calcified bone-like environment with biosynthetically active dhMSCs and niche-like 3D topology.

3.2 PCa cell growth on the 3D BME

We next imaged the growth of PC3 and C4–2B PCa cells, which both were originally derived from bone metastases but display different phenotypes. However, PC3 cells represent an aggressive, neuroendocrine-like PCa variant which lack androgen receptor and prostatic serum antigen (PSA) expression and develop particularly rapid growth, whereas

C4–2B cells typify a slow growing, castration resistant adenocarcinoma [24–26]. Multicellular tumoroids were seeded onto the BME, forming small avascular lesions (Fig. 1B). Cell growth during long-term culture was measured as fluorescence intensity of stably expressed nuclear and cytoplasmic fluorophores (H2B-eGFP and DsRed2 in PC3 cells H2B-mCherry and LifeAct-GFP in C4–2B cells). Control experiments using tumoroids of known size showed high correlation ($R>0.9$) between cell number and detected aggregated fluorescence for both cytoplasmic and nuclear signal (Fig. S2), indicating reliable fluorescence-based monitoring of cell density.

PC3 and C4–2B cells attached and expanded within and along the interconnected pore network (Fig. 3C, D), yet retained a dense tumoroid core over time (Fig. 3A, B arrowheads). PC3 cells rapidly grew on both mPCL-CaP scaffolds and BME with equal efficiency and no difference in growth kinetics were observed over 9 days, according to their aggressive nature (Fig. 3C). By comparison, C4–2B tumoroids, which required 28 days of culture to achieve a similar density of colonization, showed a trend towards accelerated growth on dhMSC-conditioned BME relative to dhMSCs-free scaffolds, possibly benefitting of stromal-derived growth signals (Fig. 3D). Both cell lines retained cell-cell junctions at the tumoroid core and developed a collective, sheet-like radiary outward expansion along the BME interface, which was more effective in PC3 compared to C4–2B tumoroids (Fig. 3E, F). Thus, 3D bone organotypic scaffolds provide an environment for tumor-cell autonomous growth of PCa tumoroids originated from cell lines.

3.3 Growth of PDX-derived tumoroids in BME

Patient-derived tumors can accurately recapitulate intra- and inter-tumoral heterogeneity and offer the possibility of personalized therapy studies [27, 28]. However, patient-derived cells are difficult to propagate upon *in vitro* culture and typically are maintained as serial xenografts in immunodeficient mice, which preserve their biological and genomic integrity and diversity [29–31]. Similarly, culture of PDX-derived cells in hydrogels [8] or organoids in reconstituted basement membrane [32] has demonstrated intact molecular diversity of prostate cancer subtypes, yet these soft materials lack the composition and biomechanical properties of bone [8, 33]. To test whether the BME could support the survival and growth of explanted PDXs, we exploited two bone metastasis-derived PDXs defined as MDA PCa 183 (a treatment naïve, androgen dependent adenocarcinoma) and MDA PCa 118b (an androgen-independent, more aggressive carcinoma resistant to androgen deprivation and chemotherapy) [16–18]. PDX-derived cells were isolated from mice, enriched by density gradient centrifugation (Fig. S3) and subjected to long-term *in vitro* culture (Fig. 4A). For fluorescence detection, freshly isolated PDX-derived cells were lentivirally transduced to express mCherry fluorescent protein (Fig. S3, 4A).

After seeding, MDA PCa 118b cells initially generated small colonies that grew for up to 50 days and expanded almost 10 times in the BME, which was in line with their more aggressive nature, while no cells survived when MDA PCa 118b PDX was cultured in the absence of dhMSCs (Fig. 4B). Tumor cells, identified by cytokeratin 8/18 positivity (Fig. 4C), grew as multifocal nests surrounded by dhMSCs and retained compact epithelial organization (Fig. 4D), similar to their organization in bone, *in vivo* (Fig. 4H). MDA PCa

183 cells initially attached as larger multicellular colonies on both mPCL-CaP scaffolds and BME but survived and further grew only when stromal cells were present, with tumoroids doubling in size after 30 days (Fig. 4E). Multicellular colonies retained homogenous expression of cytokeratin 8/18 and epithelial, *in vivo*-like configuration (Fig. 4F, H) and grew as clusters anchored to the BME (Fig. 4G). Thus, 3D bone organotypic culture supports stroma-dependent growth and propagation of PDX-derived cells and maintenance of their epithelial phenotype.

3.4 The 3D BME for studying therapy response and resistance

Tumor-stroma cell-cell interactions and paracrine activation of survival pathways may impact the sensitivity of metastatic cancer cells to therapeutic compounds and even support drug resistance [4]. Alternatively, by up-regulating signaling hubs that sensitize tumor cells or accumulating bone-tropic drugs, the stromal component can also support lethality mechanisms and enhance responsiveness to therapy [4, 34]. To exploit the BME for addressing PCa therapy response and the role of the stromal compartment therein, we first applied docetaxel, a chemotherapeutic agent that stabilizes microtubules, inhibits cell-cycle progression and induces apoptosis [33] (Fig. 1C). In 2D culture docetaxel dose-dependently compromised PC3 cell growth at doses equal or higher than 1 nM and eliminated viable cells at a dose of 30 nM (Fig. 5A, B). Docetaxel induced a dose-dependent response in BME culture, however its efficacy was further linked to the presence of dhMSC, with persisting cancer cell survival in BME but not mPCL-CaP scaffolds (Fig. 5A, C). To gain insight into sub-regions, which might support this phenomenon despite docetaxel treatment, we microscopically mapped apoptosis induction in PC3 cells inside the tumoroid core and along the dhMSC interface (Fig. 5D). PC3 cells located at the interface of dhMSC-containing BME, but not mPCL-CaP scaffolds, showed significant lower nuclear fragmentation (Fig. 5E, red arrowheads), while apoptotic rates in the tumoroid core were comparable for either culture condition (Fig. 5E, green arrowheads). The viability of dhMSCs was minimally compromised by docetaxel treatment (Fig. S4), which is consistent with limited cytotoxic activity towards non-mitotic cells ([33]; compare Fig. 2F). Thus, although PC3 cell growth in the 3D bone mimetic culture does not depend on stromal cells (Fig. 3), survival during cytotoxic challenge by docetaxel benefits from the presence of a stromal component (Fig. 5E). These results suggest an active contribution of the bone stroma to PCa cell resistance to docetaxel, resulting in preferential PCa cell survival along the dhMSC-containing interface. The presence of a diverse number, distribution and nature (homo- vs. hetero-typic) of cell-cell junctions or paracrine signals might actively support the differential response to docetaxel.

Besides chemotherapy, which affects cancer cell directly, therapeutics targeting the bone stroma can control tumor growth and progression, including Radium 223 (Rad223), an alpha-emitting radio-isotope with calcium-mimetic properties that significantly prolongs overall survival in advanced metastatic PCa patients [35] [36]. We first investigated whether Rad223 differentially distributes in 2D versus BME 3D culture (Fig. 6A). In 2D culture, Rad223 remained dissolved in the supernatant, without absorbance to the culture dish (Fig. 6B). In BME, however, Rad223 was near-completely (> 90%) detected in the scaffold and

diminished from the supernatant (Fig. 6B), consistent with its bone-tropic localization *in vivo* [37].

In 2D culture, Rad223 effects followed a near-linear dose-response with 20, 45 and >95% reduction of cell numbers for respective doses of 200, 400 and >1600 Bq/ml (Fig. 6C). In BME culture, however, Rad223 was more efficient, requiring almost ten-fold lower concentration (25 Bq/ml) to compromise PCa cell growth, and reached maximum efficacy at 200Beq/ml without further increase at higher dose (Fig. 6D, E). Nuclear fragmentation rates were low in cancer cells localized on top of the tumoroid core and significantly increased in PC3 cells along the dhMSC-interface (Fig. 6F, G), consistent with a differential exposure to Rad223, which is maximized at the interface and diminishes with greater distance due to limited penetration of alpha particles (~100 μm [34]).

These data indicate that BME culture supports both local enrichment of Rad223 to the calcified bone-mimetic compartment and a locally confined therapy response of PCa tumoroids near the dhMSC-interface.

4. Discussion and conclusions

The engineered BME provides central bone features and enables mechanistic, three-dimensional and time-resolved analysis of (i) positioning and function of PCa cells, (ii) their interaction with calcified bone stroma and osteoblasts, (iii) and the consequences for the sensitivity to chemo- and radiotherapy. The BME combines engineered, micro-sized scaffolds consisting of mPCL-CaP fibers functionalized with stromal cells that deposit calcium and distribute in a niche-like 3D topology. This system, which recapitulates principal features of calcified bone for co-culture with tumor cells, is amenable for live-cell and high-resolution fluorescence microscopy to discern types of cell-autonomous versus stroma-dependent growth. As potential biotechnological advance, besides established PCa cell lines, the BME supports organotypic retention of epithelial growth by PDX cells over weeks. Compared to other culture strategies for patient-derived cells, including 3D organoids in reconstituted basement membrane [32], the tumoroids in the BME are maintained in the presence of both extracellular matrix and a bioactive stroma. Thus, PCa cells growth and response to cytotoxic therapy in BME may be mediated by dhMSC-derived extracellular collagenous matrix and calcium deposits, paracrine signals released by stromal cells [10] and heterotypic cell-cell interactions [8].

In vivo analyses in small animals have identified key steps of the complex progression of bone metastasis, including cancer cell extravasation, survival and colonization [38–40]. *In vivo* systems however lack the fine control of the experimental variables, including topological, physical and molecular cues, and impose significant experimental and logistic demands, including animal welfare issues [41]. On the other hand, 2D cultures are simple, consistent and readily reproducible, but limited in their complexity and unable to replicate tissue-specific pathophysiology [42]. The 3D biomimetic models thus fill a technical gap between conventional 2D approaches and preclinical *in vivo* models. In principle, 3D biomimetic systems are not supposed to fully reproduce all the aspects of the bone tissue or the metastatic process, but are expected to recapitulate the essential elements and functions

needed to address relevant preclinical and clinical questions. As an example, research in a microfluidic bone-like microenvironment identified the CXCR2-CXCL5 axis as a mediator of breast cancer cells extravasation [43] and a 3D indirect co-culture model of PCa cells and osteoblasts revealed paracrine regulation of osteomimicry and androgen-responsive genes [10]. Thus, bone-mimetic systems contribute to clarify defined aspects of the complex spatial cellular and molecular interactions occurring between cancer and bone stromal cells [6].

Beyond application in PCa propagation, the bioactive BME is particularly suitable to investigate the response to therapeutic agents and the role of the bone stroma in either limiting or enhancing their efficacy. We here show that PCa cell culture in 3D osteoblastic bone stroma supports chemoresistance, consistent with *in vivo* evidence showing that osteoblasts protect cancer cells from toxicity induced by chemo- and molecular therapeutics [44, 45]. On the other hand, the BME absorbs Rad223, thus recapitulating its bone-seeking properties *in vivo* [37]. Thus, the consistency of our results with *in vivo* findings further validates the BME as a promising model that enables the dissection of tumor-stroma axis in response to therapy and mechanisms of resistance.

To extend its applicability, the BME stroma is amenable to further enrichment by endothelial cells forming vascular structures, osteoclasts contributing to matrix remodeling, adipocytes and/or bone marrow stem cells and immune cells providing additional paracrine conditioning. When applied towards PDX- or patient-derived cells the BME will enhance personalized medicine and co-clinical analysis to better establish and predict the heterogeneity and efficacy of anti-cancer therapy.

Supplementary Material

Refer to Web version on PubMed Central for supplementary material.

Acknowledgements

We thank Prof. Dietmar W. Hutmacher and Dr. Elena M. De-Juan-Pardo for scaffold generation (Institute of Health and Biomedical Innovation, Queensland University, Brisbane, Australia); Peter Shepherd (the University of Texas, MD Anderson Cancer Center, Houston, TX, USA) for providing PDXs used for propagation. E.D. is supported by the Cancer Prevention and Research Institute of Texas (RP140482), TX, USA, the Prostate Cancer Foundation (16YOUN24), CA, USA and The Rolanette and Berdon Lawrence Bone Disease Program of Texas, TX, USA; P.F. is supported by NWO-VICI (918.11.626), the European Research Council (ERC-CoG DEEPINSIGHT, Project No. 617430), the Cancer Genomics Cancer, The Netherlands; E.D., P.F. and N.N are supported by the Prostate Cancer Moonshot Program at MD Anderson Cancer Center. The Genitourinary Cancers Program of the Cancer Center Support Grant (CCSG) shared resources at MD Anderson Cancer Center was supported by NIH/NCI award number P30 CA016672.

References

[1]. Weilbaecher KN, Guise TA, McCauley LK. Cancer to bone: a fatal attraction. Nat Rev Cancer. 2011;11:411–25. [PubMed: 21593787]

[2]. Croucher PI, McDonald MM, Martin TJ. Bone metastasis: the importance of the neighbourhood. Nat Rev Cancer. 2016;16:373–86. [PubMed: 27220481]

[3]. Ellem SJ, De-Juan-Pardo EM, Risbridger GP. In vitro modeling of the prostate cancer microenvironment. Advanced drug delivery reviews. 2014;79–80:214–21.

[4]. McMillin DW, Negri JM, Mitsiades CS. The role of tumour-stromal interactions in modifying drug response: challenges and opportunities. Nat Rev Drug Discov. 2013;12:217–28. [PubMed: 23449307]

[5]. Fischbach C, Chen R, Matsumoto T, Schmelzle T, Brugge JS, Polverini PJ, et al. Engineering tumors with 3D scaffolds. Nat Methods. 2007;4:855–60. [PubMed: 17767164]

[6]. Salamanna F, Contartese D, Maglio M, Fini M. A systematic review on in vitro 3D bone metastases models: A new horizon to recapitulate the native clinical scenario? Oncotarget. 2016;7:44803–20. [PubMed: 27027241]

[7]. Sung SY, Hsieh CL, Law A, Zhau HE, Pathak S, Multani AS, et al. Coevolution of prostate cancer and bone stroma in three-dimensional coculture: implications for cancer growth and metastasis. Cancer Res. 2008;68:9996–10003. [PubMed: 19047182]

[8]. Fong EL, Wan X, Yang J, Morgado M, Mikos AG, Harrington DA, et al. A 3D in vitro model of patient-derived prostate cancer xenograft for controlled interrogation of in vivo tumor-stromal interactions. Biomaterials. 2016;77:164–72. [PubMed: 26599623]

[9]. Talukdar S, Kundu SC. Engineered 3D Silk-Based Metastasis Models: Interactions Between Human Breast Adenocarcinoma, Mesenchymal Stem Cells and Osteoblast-Like Cells. Adv Funct Mater. 2013;23:5249–60.

[10]. Sieh S, Taubenberger AV, Lehman ML, Clements JA, Nelson CC, Hutmacher DW. Paracrine interactions between LNCaP prostate cancer cells and bioengineered bone in 3D in vitro culture reflect molecular changes during bone metastasis. Bone. 2014;63:121–31. [PubMed: 24530694]

[11]. Jeon JS, Bersini S, Gilardi M, Dubini G, Charest JL, Moretti M, et al. Human 3D vascularized organotypic microfluidic assays to study breast cancer cell extravasation. Proc Natl Acad Sci U S A. 2015;112:214–9. [PubMed: 25524628]

[12]. Curtin P, Youm H, Salih E. Three-dimensional cancer-bone metastasis model using ex-vivo co-cultures of live calvarial bones and cancer cells. Biomaterials. 2012;33:1065–78. [PubMed: 22071100]

[13]. Elliott NT, Yuan F. A review of three-dimensional in vitro tissue models for drug discovery and transport studies. J Pharm Sci. 2011;100:59–74. [PubMed: 20533556]

[14]. Fitzgerald KA, Guo J, Tierney EG, Curtin CM, Malhotra M, Darcy R, et al. The use of collagen-based scaffolds to simulate prostate cancer bone metastases with potential for evaluating delivery of nanoparticulate gene therapeutics. Biomaterials. 2015;66:53–66. [PubMed: 26196533]

[15]. Subia B, Dey T, Sharma S, Kundu SC. Target specific delivery of anticancer drug in silk fibroin based 3D distribution model of bone-breast cancer cells. ACS Appl Mater Interfaces. 2015;7:2269–79. [PubMed: 25557227]

[16]. Li ZG, Mathew P, Yang J, Starbuck MW, Zurita AJ, Liu J, et al. Androgen receptor-negative human prostate cancer cells induce osteogenesis in mice through FGF9-mediated mechanisms. J Clin Invest. 2008;118:2697–710. [PubMed: 18618013]

[17]. Roychowdhury S, Iyer MK, Robinson DR, Lonigro RJ, Wu YM, Cao X, et al. Personalized oncology through integrative high-throughput sequencing: a pilot study. Sci Transl Med. 2011;3:111ra21.

[18]. Navone NLE. Patient-Derived Xenograft Models of Human Cancer. Humana Press 2017:93–114.

[19]. Martine LC, Holzapfel BM, McGovern JA, Wagner F, Quent VM, Hesami P, et al. Engineering a humanized bone organ model in mice to study bone metastases. Nat Protoc. 2017;12:639–63. [PubMed: 28253234]

[20]. Schneider CA, Rasband WS, Eliceiri KW. NIH Image to ImageJ: 25 years of image analysis. Nature methods. 2012;9:671–5. [PubMed: 22930834]

[21]. Dondossola E, Holzapfel BM, Alexander S, Filippini S, Hutmacher DW, Friedl P. Examination of the foreign body response to biomaterials by nonlinear intravital microscopy. Nat Biomed Eng. 2016;1.

[22]. Ruminski S, Ostrowska B, Jaroszewicz J, Skirecki T, Wlodarski K, Swieszkowski W, et al. Three-dimensional printed polycaprolactone-based scaffolds provide an advantageous environment for osteogenic differentiation of human adipose-derived stem cells. J Tissue Eng Regen Med. 2016.

[23]. Rai B, Lin JL, Lim ZX, Guldberg RE, Hutmacher DW, Cool SM. Differences between in vitro viability and differentiation and in vivo bone-forming efficacy of human mesenchymal stem cells cultured on PCL-TCP scaffolds. Biomaterials. 2010;31:7960–70. [PubMed: 20688388]

[24]. Thalmann GN, Anezinis PE, Chang SM, Zhau HE, Kim EE, Hopwood VL, et al. Androgen-independent cancer progression and bone metastasis in the LNCaP model of human prostate cancer. Cancer Res. 1994;54:2577–81. [PubMed: 8168083]

[25]. Tai S, Sun Y, Squires JM, Zhang H, Oh WK, Liang CZ, et al. PC3 is a cell line characteristic of prostatic small cell carcinoma. The Prostate. 2011;71:1668–79. [PubMed: 21432867]

[26]. Kaighn ME, Narayan KS, Ohnuki Y, Lechner JF, Jones LW. Establishment and characterization of a human prostatic carcinoma cell line (PC-3). Invest Urol. 1979;17:16–23. [PubMed: 447482]

[27]. Rea D, Del Vecchio V, Palma G, Barbieri A, Falco M, Luciano A, et al. Mouse Models in Prostate Cancer Translational Research: From Xenograft to PDX. Biomed Res Int. 2016;2016:9750795. [PubMed: 27294148]

[28]. Sheth RA, Perkons N, Dondossola E, Subudhi SK, Gade TP, Tam AL Patient-Derived Xenograft Tumor Models: Overview and Relevance to IR. JVIR. 2018;29:880–2. [PubMed: 29798759]

[29]. Risbridger GP, Toivanen R, Taylor RA. Preclinical Models of Prostate Cancer: Patient-Derived Xenografts, Organoids, and Other Explant Models. Cold Spring Harb Perspect Med. 2018.

[30]. Lin D, Wyatt AW, Xue H, Wang Y, Dong X, Haegert A, et al. High fidelity patient-derived xenografts for accelerating prostate cancer discovery and drug development. Cancer Res. 2014;74:1272–83. [PubMed: 24356420]

[31]. Siolas D, Hannon GJ. Patient-derived tumor xenografts: transforming clinical samples into mouse models. Cancer Res. 2013;73:5315–9. [PubMed: 23733750]

[32]. Gao D, Vela I, Sboner A, Iaquinta PJ, Karthaus WR, Gopalan A, et al. Organoid cultures derived from patients with advanced prostate cancer. Cell. 2014;159:176–87. [PubMed: 25201530]

[33]. Montero A, Fossella F, Hortobagyi G, Valero V. Docetaxel for treatment of solid tumours: a systematic review of clinical data. Lancet Oncol. 2005;6:229–39. [PubMed: 15811618]

[34]. Bruland OS, Nilsson S, Fisher DR, Larsen RH. High-linear energy transfer irradiation targeted to skeletal metastases by the alpha-emitter 223Ra: adjuvant or alternative to conventional modalities? Clin Cancer Res. 2006;12:6250s–7s. [PubMed: 17062709]

[35]. Parker C, Nilsson S, Heinrich D, Helle SI, O'Sullivan JM, Fossa SD, et al. Alpha emitter radium-223 and survival in metastatic prostate cancer. N Engl J Med. 2013;369:213–23. [PubMed: 23863050]

[36]. Suominen MI, Rissanen JP, Kakonen R, Fagerlund KM, Alhoniemi E, Mumberg D, et al. Survival benefit with radium-223 dichloride in a mouse model of breast cancer bone metastasis. J Natl Cancer Inst. 2013;105:908–16. [PubMed: 23682134]

[37]. Abou DS, Ulmert D, Doucet M, Hobbs RF, Riddle RC, Thorek DL. Whole-Body and Microenvironmental Localization of Radium-223 in Naive and Mouse Models of Prostate Cancer Metastasis. J Natl Cancer Inst. 2016;108.

[38]. Shiozawa Y, Pedersen EA, Havens AM, Jung Y, Mishra A, Joseph J, et al. Human prostate cancer metastases target the hematopoietic stem cell niche to establish footholds in mouse bone marrow. J Clin Invest. 2011;121:1298–312. [PubMed: 21436587]

[39]. Wang B, Lai X, Price C, Thompson WR, Li W, Quabili TR, et al. Perlecan-containing pericellular matrix regulates solute transport and mechanosensing within the osteocyte lacunar-canalicular system. J Bone Miner Res. 2014;29:878–91. [PubMed: 24115222]

[40]. Shiozawa Y, Pedersen EA, Patel LR, Ziegler AM, Havens AM, Jung Y, et al. GAS6/AXL axis regulates prostate cancer invasion, proliferation, and survival in the bone marrow niche. Neoplasia. 2010;12:116–27. [PubMed: 20126470]

[41]. Landgraf M, McGovern JA, Friedl P, Hutmacher DW. Rational Design of Mouse Models for Cancer Research. Trends Biotechnol. 2018;36:242–51. [PubMed: 29310843]

[42]. Cunningham D, You Z. In vitro and in vivo model systems used in prostate cancer research. J Biol Methods. 2015;2.

[43]. Bersini S, Jeon JS, Dubini G, Arrigoni C, Chung S, Charest JL, et al. A microfluidic 3D in vitro model for specificity of breast cancer metastasis to bone. Biomaterials. 2014;35:2454–61. [PubMed: 24388382]

[44]. Zheng H, Bae Y, Kasimir-Bauer S, Tang R, Chen J, Ren G, et al. Therapeutic Antibody Targeting Tumor- and Osteoblastic Niche-Derived Jagged1 Sensitizes Bone Metastasis to Chemotherapy. Cancer Cell. 2017;32:731–47 e6. [PubMed: 29232552]

[45]. Yu KJ, Li JK, Lee YC, Yu G, Lin SC, Pan T, et al. Cabozantinib-induced osteoblast secretome promotes survival and migration of metastatic prostate cancer cells in bone. Oncotarget. 2017;8:74987–5006. [PubMed: 29088840]

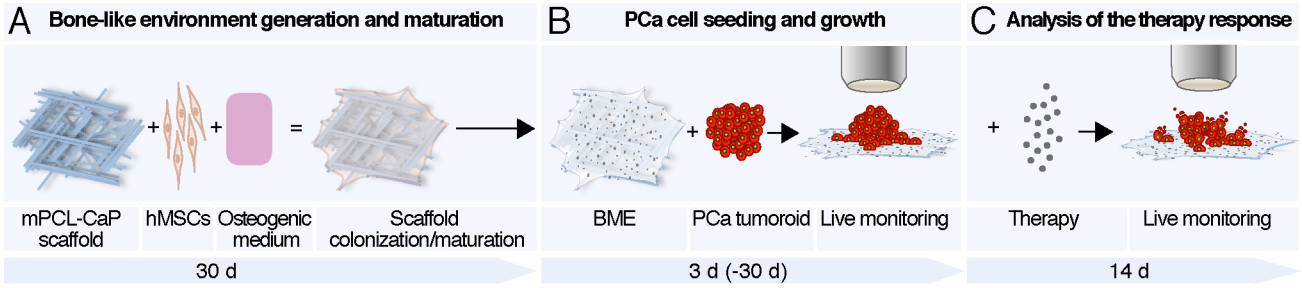

Fig. 1. Schematic representation of the bone mimetic environment of metastasis.

A. Human mesenchymal stem cells (hMSCs) were seeded on a miniaturized medical grade, calcium phosphate polycaprolactone scaffold (mPCL-CaP) and maintained in osteogenic medium for 30 days that engendered osteogenic maturation. **B**. PCa cells were seeded on the bone mimetic environment (BME) as tumoroids and monitored over time by live-cell fluorescence microscopy. **C**. Established tumoroids were subjected to chemo- or radiation therapy and longitudinally monitored for therapeutic response by live-cell fluorescence microscopy.

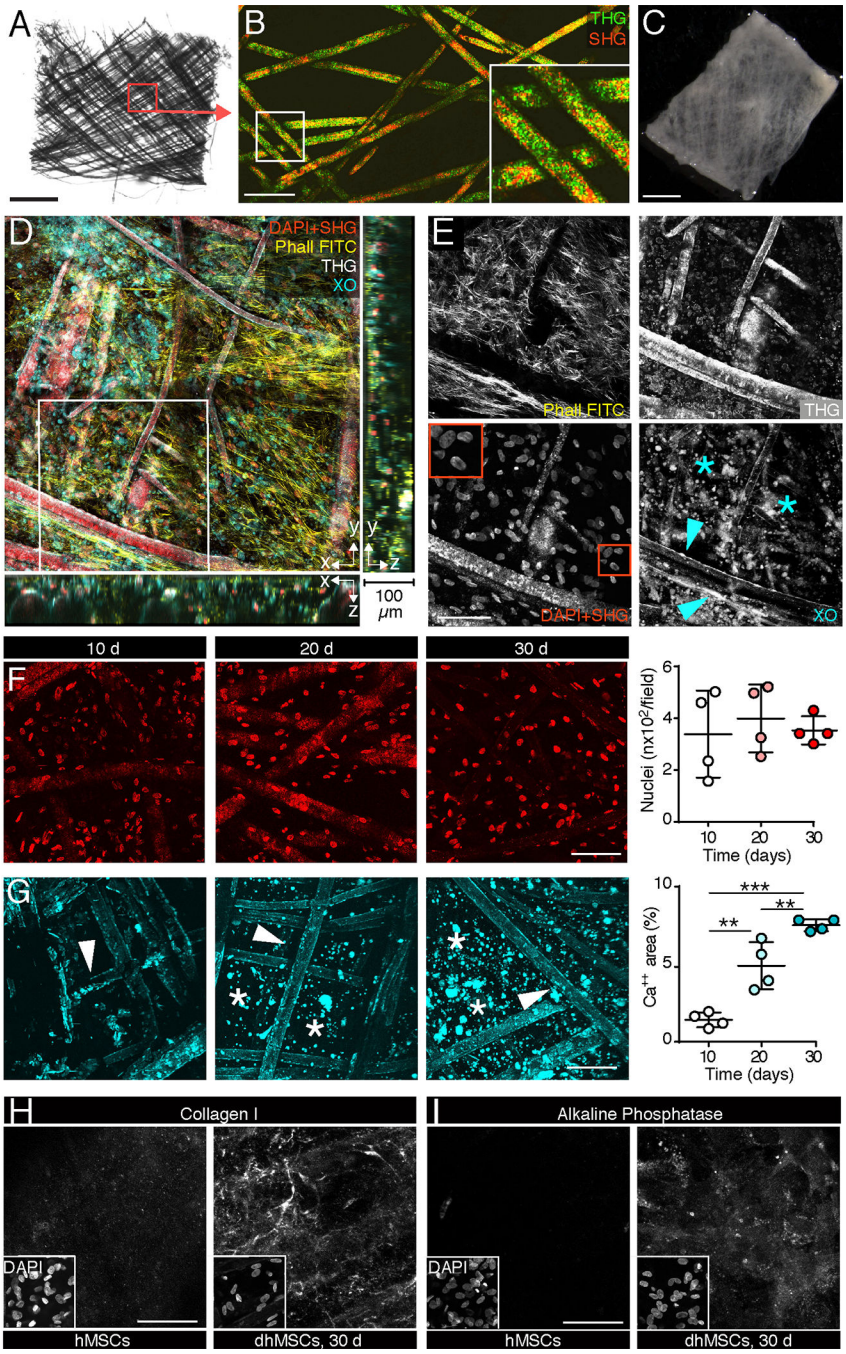

Fig. 2. Maturation of the *in vitro* engineered bone-like microenvironment monitored by non-linear microscopy.

A. Topology of native mPCL-CaP scaffold (bright field microscopy). Bar, 1 mm. **B**. 3D organization of native mPCL fibers detected by second and third harmonic generation (SHG, THG) microscopy. Box, region of single-channel images. Bar, 150 μm. **C**. mPCL-CaP scaffold functionalized with hMSCs after 30 days of osteogenic culture (overview, bright field microscopy). Bar, 150 μm. **D**, **E**. 3D organization of the engineered bone-like microenvironment 30 days after hMSCs seeding, detected by multiphoton microscopy.

Merged and single channel images are shown. Red box, inset with nuclei; arrowhead, calcium deposited on the fibers; asterisk, inter-fiber calcium deposits. DAPI, SHG, red; phalloidin, yellow; xylenol orange, Cyan; THG, White. Bar, 100 μm; z-depth 100 μm. **F**. Quantification of nuclei number over time; means ± SD, 4 biological replicates. **G**. Quantification of calcium deposition over time stained by xylenol orange. Arrowhead, calcium deposited on the fibers; asterisk, calcium deposited inter-fibers; means ± SD, 4 biological replicates. (**F**, **G**) (**) $p<0.01$, (***) $p<0.001$, one-way Anova and Tukey's post hoc test. Bar, 100 μm. **H**, **I**. Staining of collagen I and alkaline phosphatase on functionalized scaffolds before and after the differentiation process (differentiated human mesenchymal stem cells, dhMSCs; 30 days). White box, inset with nuclei. Bar, 50 μm.

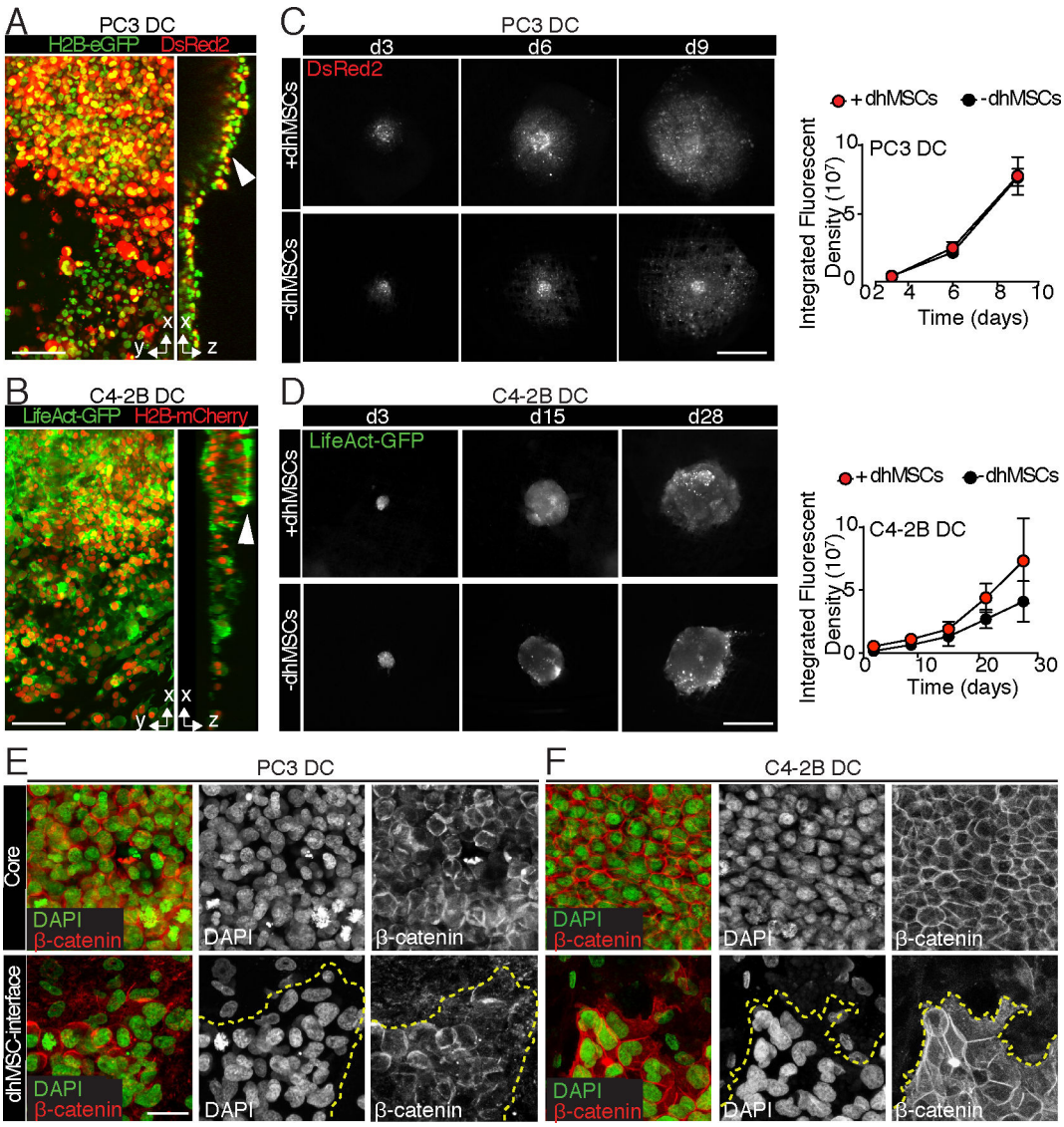

Fig. 3. Growth of PCa tumoroids on functionalized and mPCL-CaP scaffolds.

A, **B**. 3D reconstruction and x-z orthogonal view by multiphoton microscopy of PC3 DC (**A**) and C4–2B DC (**B**) tumoroids. Bar, 100 μm. Arrowhead, tumoroids core. **C, D**. PC3 DC (**C**) and C4–2B DC (**D**) tumoroids on BME and mPCL-CaP scaffolds detected by epifluorescence microscopy. Quantification of growth kinetics is shown (PC3 DC: DsRed2; C4–2B: LifeAct-GFP), means ± SD from 3 independent experiments with 4 scaffolds/time point. Bar, 1mm. **E**, **F**. PC3 DC (**E**) and C4–2B DC (**F**) cell-cell junctions as assessed by β-catenin staining, in both core and dhMSC-interface areas. Merged and single channel images are shown. DAPI, green; β-catenin, red. Bar, 10 μm.

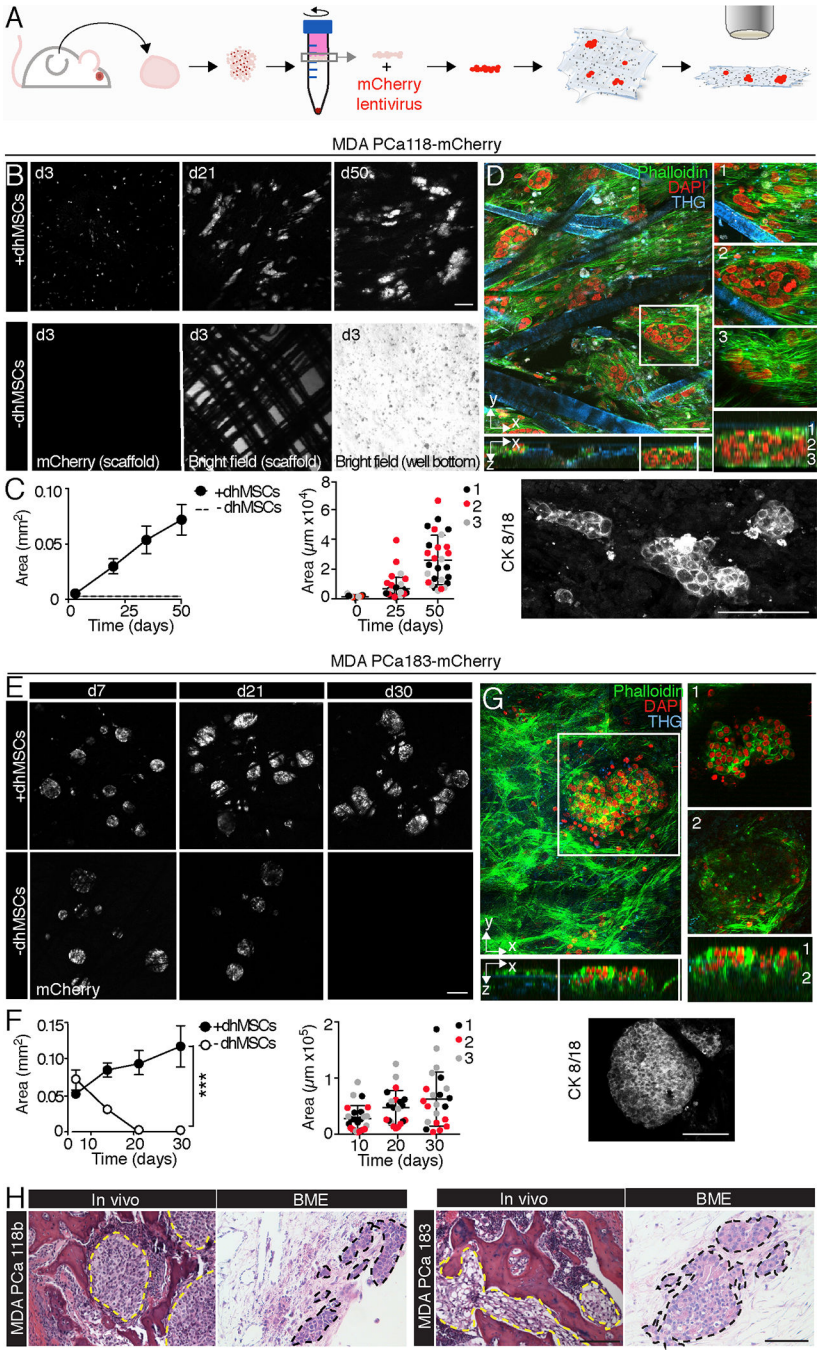

Fig. 4. MDA PCa 118b and 183 growth in bone-mimetic environment.

A. Workflow of PDX-derived BME culture. Procedures are described in Results. **B**, **C**. Time-dependent growth and distribution of MDA PCa 118b/m-Cherry colonies on BME and mPCL-CaP scaffolds. 3 independent experiments were performed, with 3 scaffolds per condition. One representative experiment is shown. Bar, 200 μm. Right panel, cytokeratin 8/18 staining of BME at day 21. Bar, 200 μm. **D**. 3D reconstruction and x-z orthogonal view of MDA PCa 118b on BME by multiphoton microscopy. White box, zoomed images representing different sections of 150 μm in z-depth (1, 2, 3). Red, DAPI; green, phalloidin;

blue, THG. Bar 100 μm. **E, F**. Time-dependent growth and distribution of MDA PCa 183/m-Cherry colonies on BME and mPCL-CaP scaffolds. Quantification of growth and size of PCa colonies overtime; 3 independent experiments were performed, with 3 scaffolds per condition; one representative experiment is shown. (***) $p<0.001$, by Student's T-test, two tailed. Bar, 200 μm. Right panel, cytokeratin 8/18 staining of BME at day 21. Bar, 200 μm. **G**. 3D reconstruction and x-z orthogonal view of MDA PCa 118b on BME by multiphoton microscopy. White box, magnification. The magnification is shown at different depth levels (1, 2; z-depth, 150 μm). Red, DAPI; green, phalloidin; blue, THG. Bar 100 μm. **H**. Histology of MDA PCa 118b and MDA PCa 183 in bone and BME. Yellow and black dashed lines outline the tumor areas. Bar, 200 μm.

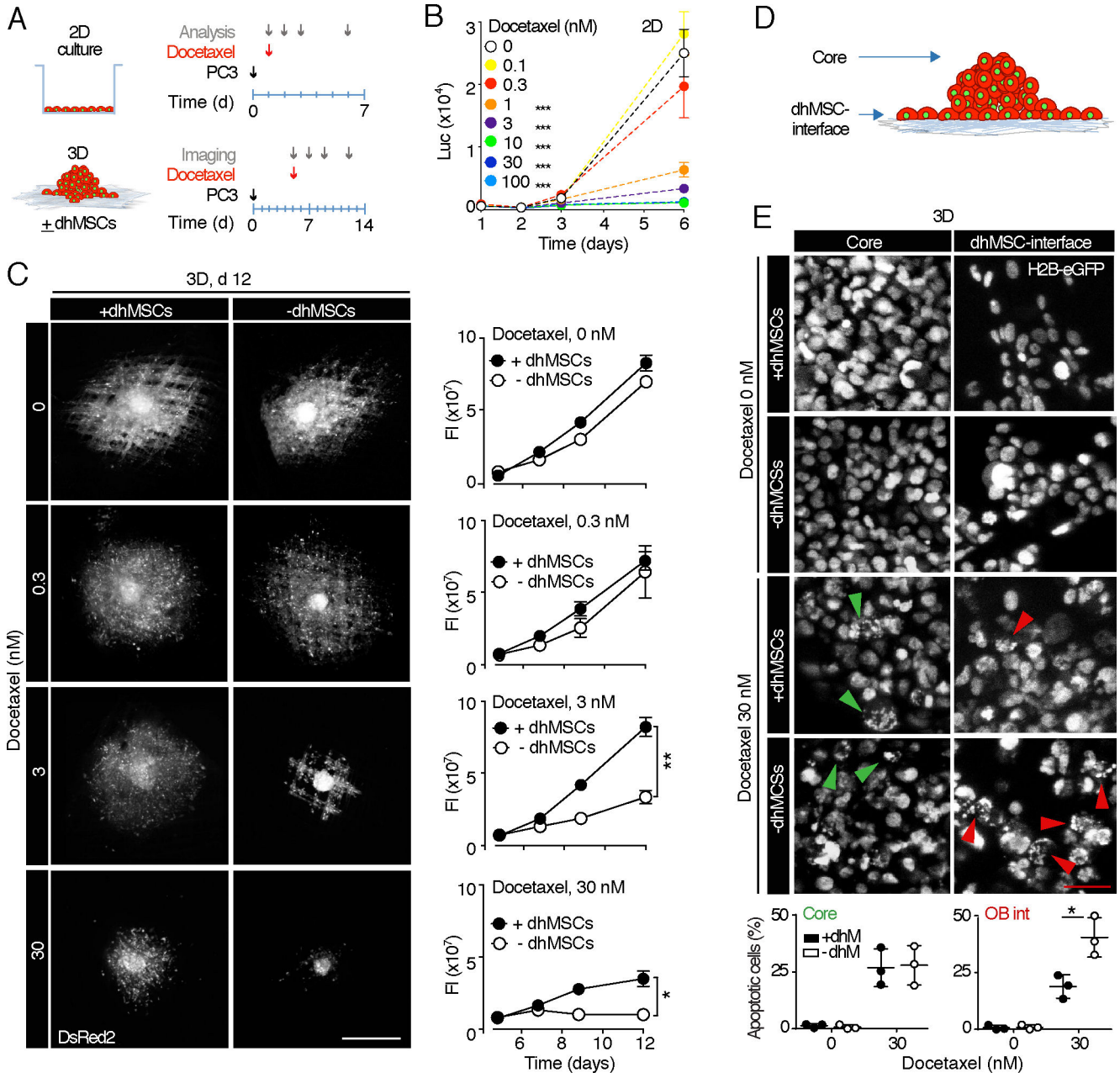

Fig. 5. PC3 2D and BME culture dose-response curve to docetaxel.

A. Time line of docetaxel treatment in 2D vs. 3D culture ± dhMSCs. **B**. Dose-response curve based on photon emission by luciferase-positive PC3 treated with docetaxel on cell culture plate. 2 independent experiments were performed, in triplicate. One representative experiment is shown, means ± SD. **C**. PC3 DC tumoroids treated with 0nM, 0.3nM, 3nM and 30nM of docetaxel at day 12, +/−dhMSCs detected by epifluorescence microscopy. Tumoroid growth was monitored by fluorescence intensity analysis. 3 independent experiments were performed, with 3 scaffolds per condition; one representative experiment is shown, means ± SD. Bar, 500 μm. (*) $p<0.05$; (**) $p< 0.01$ by Student's T-test, two tailed. **D**. Schematic representation of the tumoroids seeded on BME, showing the core and the

dhMSC-interface. **E**. PC3 DC cells (nucleus, H2B-eGFP) 2 days post-treatment with 0 or 30 nM docetaxel, in both core and dhMSC-interface areas, detected by confocal microscopy. Green arrowhead, apoptotic nuclei in the core; red arrowhead, apoptotic nuclei at the dhMSC-interface. The number of apoptotic nuclei is shown. Data represent the means ± SD from 3 independent experiments with 3 scaffolds/time point. Bar, 5 μm. (*) $p<0.05$ by Student's T-test, two tailed.

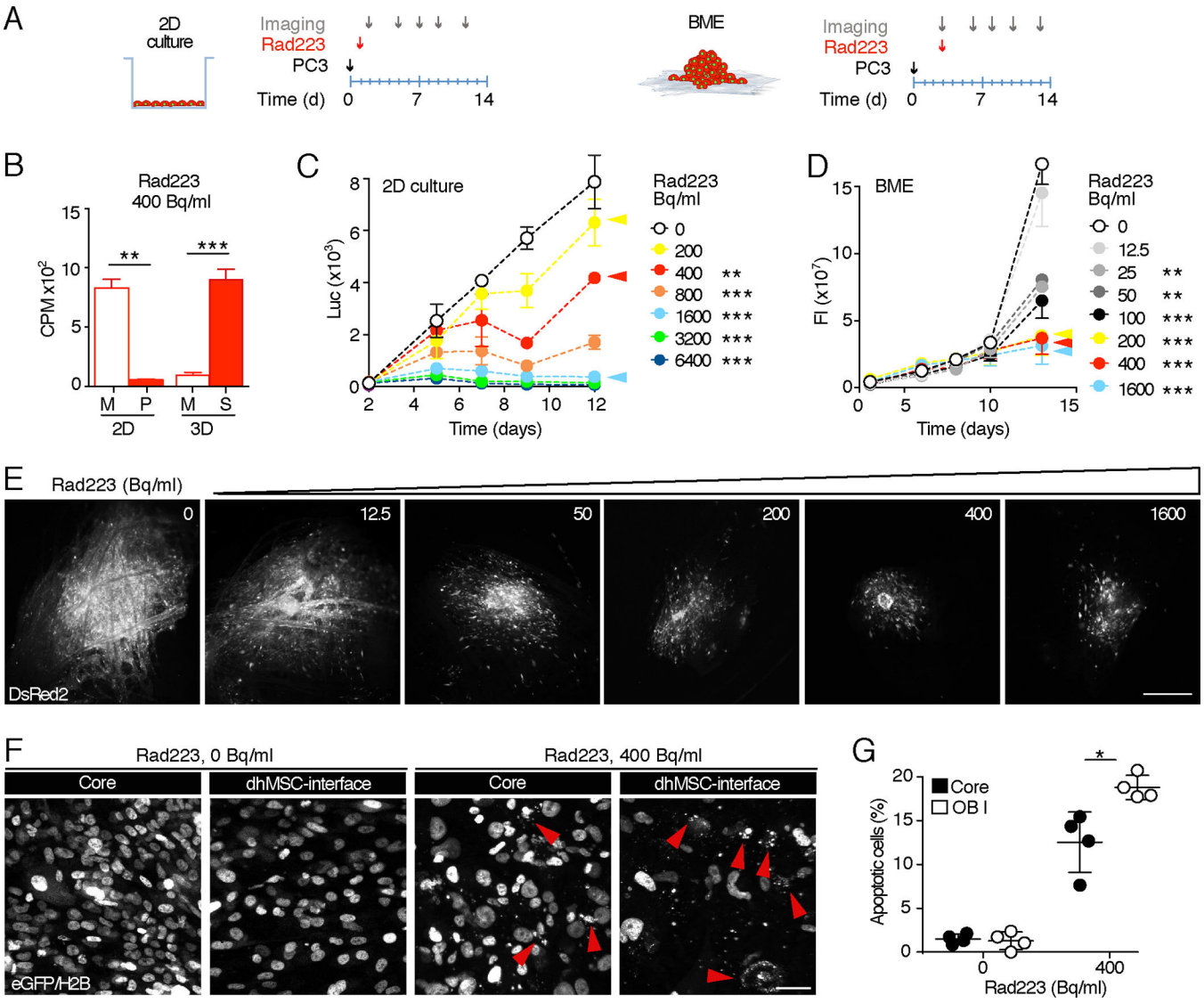

Fig. 6. PC3 2D and BME culture dose-response curve to Rad223.

A. Time line of Rad223 treatment in 2D and 3D. **B**. α-particle emission in 2D and 3D samples treated with Rad223 400 Becquerel/ml. M, medium; P, plastic; S, scaffold. (**) $p<0.01$; (***) $p< 0.001$ by Student's T-test, two tailed. **C**. Dose-response curve based on photon emission by luciferase-positive PC3 treated with Rad223 on cell culture plate. 2 independent experiments were performed, in triplicate. One representative experiment is shown, means ± SD. **D**. 3D dose-response curve of PC3 DC cells on BME treated with Rad223, monitored by fluorescence intensity analysis. Data represent the means ± SD, from 3 independent experiments with 3 scaffolds/time point. **E**. PC3 DC tumoroids detected at day 13 by epifluorescence microscopy. DsRed2 signal is shown. Bar, 500 μm. **F, G**. PC3 DC cells (nucleus, H2B-eGFP) 2 days post-treatment with 0 or 400 Bq/ml of Rad223, in both core and dhMSC-interface. Data represent the means ± SD, 4 scaffolds, detected by confocal microscopy. Bar, 5 μm. (*) $p<0.05$ by Student's T-test, two tailed.